Regular Article

PHYSICAL CHEMISTRY RESEARCH
Published by the
Iranian Chemical Society
www.physchemres.org
info@physchemres.org

Phys. Chem. Res., Vol. 10, No. 4, 519-535, December 2022
DOI: 10.22036/PCR.2022.331866.2040

In Silico Prediction of Novel (TRIM24) Bromodomain Inhibitors: A Combination of 3D-QSAR, Molecular Docking, ADMET Prediction, and Molecular Dynamics Simulation

O. Chedadi[a,*], A. El Aissouq[b], Y. El Ouardi[c], M. Bouachrined[d] and A. Ouammou[a]

[a]*LIMOME Laboratory, Faculty of Sciences Dhar El Mahraz, Sidi Mohamed Ben Abdellah University, Fez, Morocco*
[b]*Laboratory of Processes, Materials and Environment (LPME), Faculty of Science and Technology, Sidi Mohamed Ben Abdellah University, Fez, Morocco*
[c]*Laboratory of Separation Technology, Lappeenranta University of Technology, Lappeenranta, Finland*
[d]*EST Khenifra, Sultan Moulay Sliman University, Morocco*
(Received 1 March 2022, Accepted 28 March 2022)

Recently, a new series of N-benzyl-3,6-dimethylbenzo[d]-isoxazol-5-amine derivatives were produced and their prostate anti-cancer activities were evaluated. Its compounds were perceived to have a strong inhibitory effect on the bromodomain of Tripartite motif-containing protein 24 (TRIM24). The 3D-QSAR study was performed, utilizing comparative molecular field analysis (CoMFA) and comparative molecular similarity indices analysis (CoMSIA). The values of cross-validation coefficient (Q^2) were 0.850 and 0.92, and the values of determination coefficient (R^2) were 0.998 and 0.987. The predictive capacity of these models was based on a test set of seven molecules, which generated acceptable values of 0.793 and 0.804 for determination coefficient (R^2), corresponding respectively to CoMFA and CoMSIA. In This study, molecular docking analysis was used to validate the 3D-QSAR models and explain the binding site interactions and energy between the TRIM24 bromodomain receptor and the most active ligands. The results of the previous models allowed us to predict new and active compounds, and their pharmacokinetic properties were verified using drug-likeness and ADMET prediction. Finally, to affirm the dynamic stability and behavior of the molecules, the most appropriate docked candidate molecules were simulated by molecular dynamics.

Keywords: TRIM24 bromodomain, Cancer diseases, 3D-QSAR, Molecular docking, ADMET, Molecular dynamics

INTRODUCTION

Prostate cancer is a vicious non-skin cancer that attacks men all over the world. The generally adopted clinical treatment is based on androgen-deprivation, or anti-androgen, therapy, which inhibits the androgen synthesis or blocks androgen receptors (AR) signaling pathways [1,2]. In most cases, castration and anti-androgenic treatments are administered [3]. Unfortunately, the majority of patients end up developing both castration-resistant and antiandrogen-resistant prostate cancers [4]. Because castration-resistant prostate cancer (CRPC) is often fatal, CRPC patients need more effective targeted therapy drugs. Consequently, in the past few years, abundant research has focused on developing molecule inhibitors of nuclear receptors in CRPC, along with small molecules inhibiting BCP (bromodomain-containing protein) [5-7]. In the present study, the authors identified the Tripartite motif-containing protein 24 (TRIM24) among the target proteins [8].

TRIM24, also called transcription intermediary factor 1-alpha (TIF1α) [9], is a multifunctional protein which

*Corresponding author. E-mail: oussama.chedadi@usmba.ac.ma

plays a primordial role in various biological processes, such as homogeneous or heterogeneous polymerization [10] and ubiquitylation [11]. TRIM24 functions as a co-regulator of the transcription and binds to nuclear receptors (NRs) through its LXXLL motif [12].

Another crucial domain of TRIM24 is the bromodomain, which determines the sum of the superfamily bromodomain-containing protein (BCP) and contains sixty-one members segmented into eight groups based on the similarity of structure/sequence [13].

Having a histone epigenetic reader, TRIM24 belongs to the fifth sub-family and is capable of particularly recognizing the H3K23 acetyls (H3K23ac) through an intermediator of its bromodomain. TRIM24 binds to chromatin and estrogen receptors to activate genes that depend on estrogens and are associated with cellular proliferation and tumor development [14]. Other research indicates that TRIM24 affects carcinogenesis or tumor development in a variety of cancers, most notably prostate cancer [15].

Highly influential studies support that TRIM24 mediates the growth of CRPC *via* its bromodomains and the LXXLL motif. These studies also suggest that bromodomain is a possible medicinal target [16]. To treat CRPC, it is essential to significantly advance our understanding of the therapeutic potential of the bromodomain inhibitor TRIM24 by identifying new specific potent inhibitors.

Recently, a novel series of N-benzyl-3,6-dimethylbenzo[d]-isoxazol-5-amine derivatives have been synthesized and their anti-cancer activities have been assessed [17]. It was observed that these compounds exhibited strong inhibition against TRIM24-related bromodomains, indicating their high potential for development as a new class of medicine for the treatment of prostate cancers. Despite significant advancements in experimental research, few theoretical studies have been carried out on how the structural properties of these compounds impact their anticancer activities, and the inhibitory mechanisms of these compounds targeting TRIM24 bromodomain remain largely unknown.

As one of the most efficient approaches to understanding the mechanism action of drugs and designing new drugs, the QSAR methodology consists of a quantitative correlation of the molecular structures or properties with variations in biological activity [18,19]. Moreover, molecular docking is an effective tool for calculating detailed protein-ligand interactions and obtaining 3D graphical information for a deeper conceptualization of molecular binding mode [20]. Currently, 3D-QSAR approaches that include CoMFA and CoMSIA studies are efficiently employed to understand the pharmacological characteristics of the studied compounds and design new drugs [18]. 3D-QSAR analyses elucidate both favorable and unfavorable zones impacting biological activity. Additionally, molecular docking can offer various orientations of the ligands inside the active region, which, in turn, helps researchers to hypothesize about the probable receptor-ligand interactions [19]. In this work, a novel series of N-benzyl-3,6-dimethylbenzo[d]-isoxazol-5-amine derivatives, acting as three-targeted TRIM24 bromodomain inhibitors, were produced to conduct a theoretical study utilizing 3D-QSAR and molecular docking methods. The orientations and the probable binding conformations of the composites interacting with TRIM24 bromodomain were determined and located, and 3D-QSAR models were established. Also, the predicted compounds were tested by ADMET prediction to evaluate their pharmacokinetic and pharmacodynamic properties [20,21]. To affirm the binding stability and the conformational space of the final candidate molecules, the most appropriate docked compounds were simulated by MD (molecular dynamics) [22].

We anticipate that the obtained results will be a valuable theoretical guide for the logical design of selective and innovative TRIM24 bromodomain inhibitors. Furthermore, it is hoped that the findings of this study will provide some relevant references for future experimental studies.

TOOLS AND METHODS

Data Sets

A dataset of N-benzyl-3,6-dimethylbenzo[d]-isoxazol-5-amine derivatives (30 compounds) selected from the literature based on the biological assay method was used as TRIM24 bromodomain inhibitors, synthesized, and used to generate 3D-QSAR models and conduct molecular docking analysis [17]. The dependent variable in the CoMFA and CoMSIA model was pIC50 (-logIC50), which was transformed from the activity levels (IC50 in nM) [23]. The

arbitrary partition of a training set (24 compounds, 80%) and a test set (6 compounds, 20%) were used to develop and validate the QSAR model (Table 1)

3D-QSAR Study

Molecular database optimization and alignment. The design, molecular optimization, and alignment of the 3D-QSAR model were conducted utilizing the computer package SYBYL-X 2.1 [24]. This software utilizes optimized geometry using the Tripos force field and is based on the following criteria:

- 0.001 kcal mol^{-1} as the convergence criterion,
- A maximum of 10000 repetitions,
- The Gasteiger-Hücke model is used to determine atomic charges [25].

In SYBYL-X 2.1, compound 4, which was the most active compound, was utilized as a model to align all molecules in the database.

The CoMFA Model

The CoMFA method requires arranging the individual compounds on a 2.0 Å spacing grid lattice [26]. An sp3 carbon atom with a +1 charge was utilized to examine the electrostatic (Coulombic) and steric (Lennard-Jones) field energies. The interaction energy cutoff was set at 30 kcal mol^{-1}. To reduce computing time without impacting the accuracy of the CoMFA models, column filtering was used based on the calculation of molecular-field energies with a variation smaller than 2.0 kcal mol^{-1} [27].

The robustness of the partial-least-squares (PLS) analysis was assessed by leave-one-out (LOO) cross-validation in the CoMFA methodology (LOO). For the 3D-QSAR to be statistically reliable and predictable, the cross-validation coefficient Q^2 and the correlation coefficient R^2 must be more than 0.5 and 0.6, respectively.

For the CoMFA model to be totally accurate, the standard error estimate (SEE) and the Fisher coefficient of R2 must be obtained using PLS through a non-cross validation approach. The suggested model predictive ability was validated with external validation (test set) [28].

The CoMSIA Model

The CoMSIA [29] model is the developed version of the CoMFA method.

The hydrophobic field, electrostatic field, and hydrogen-bond acceptor and donor of the CoMSIA model are as follows:

- The calculations were estimated in a 2,0 Å grid;
- The cutoff energy of the interactions was in the order of 30 kcal mol^{-1} [30];
- The attenuation factor was set at 0.3. Column filtering was based on calculating molecular-field energies that differed by less than 2.0 kcal mol^{-1}.

Molecular Docking Study

Molecular docking is a computational method for detecting and visualizing potential interactions between ligands (N-benzyl-3,6-dimethylbenzo[d]-isoxazol-5-amine derivatives) and receptors (TRIM24 bromodomain). In terms of docking processes, the suitable protein (*i.e.*, TRIM24 bromodomain) [31] was found in the Protein Data Bank [32] (PDB ID: 4YBT). The initial ligand and water molecules were eliminated, and the active site of the protein was found using the AutoDockTools [33]. A cubic grid box (X = 38, Y = 36, and Z = 28 at 0.375) was built through the re-docking of the basic ligand.

Finally, the most potent compounds and inhibitors in the active zone of the protein 4YBT were identified. The results are shown using PyMol [34] and Discovery Studio (2017) [35].

MD Simulation

Molecular dynamic (MD) simulation has shown to be a vital instrument in claiming the time-dependent stability of ligand into the active site of a protein. The best-scored complex of TRIM24 bromodomain (PDB ID: 4YBT) subsequently underwent a molecular docking study. GROMACS version 1-1 [36] was used to perform all computations.

The following parameters were used to build the MD simulation model in GROMACS:

- The CHARMM General Force Field (CGenFF) server [37] produced the topology file for the compounds whereas the 'pdb2gmx' tool created the topology file for the protein TRIM24 bromodomain (PDB ID: 4YBT);
- The simulations were carried out in a triclinic box with a distance of 1.0 nm, and a TIP3P water model solvated the system [38] using the CHARMM36 all-atom force

Table 1. The Experimental Biological Activity Dataset of Alkyl Linkers of N-benzyl-3,6-dimethylbenzo[d]-isoxazol-5-amine Derivatives

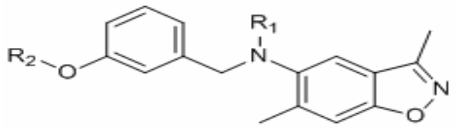

Compound	R1	R2	IC_{50} (nM) Alphascreen	pIC_{50} Alphascreen	Compound	R1	R2	IC_{50} (nM) Alphascreen	pIC_{50} Alphascreen
1	H	CH3	7.3	5.1366	16	H	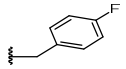	78.36	4.1059
2	H	H	7.37	5.1325	17	H		65.05	4.1867
3 [T]	H		3.84	5.4156	18	H	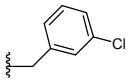	76.09	4.1186
4	H	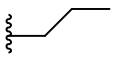	1.88	5.7258	19	H		76.41	4.1168
5	H	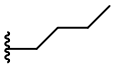	4.19	5.3777	20 [T]	H	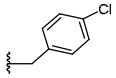	24.15	4.6170
6	H	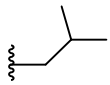	3.34	5.4762	21	H	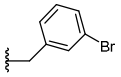	87.31	4.0589
7	H	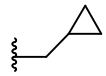	3.47	5.4596	22	H	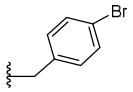	54.49	4.2636
8 [T]	H	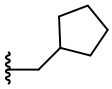	2.53	5.5968	23	H	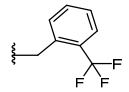	64.42	4.1909
9 [T]	H	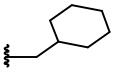	12.22	4.9129	24	H	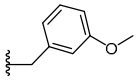	8.42	5.0746
10	H	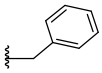	2.86	5.5436	25	H	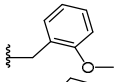	2.57	5.5900
11	H	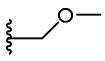	9.01	5.0452	26	H		2.33	5.6326
12	H		4.3	5.3665	27			32.79	4.4842
13	H	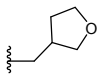	2.54	5.5951	28		H	34.19	4.4661
14 [T]	H	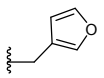	2.72	5.5654	29 [T]		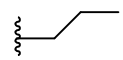	34.97	4.4563
15	H	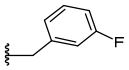	70.76	4.1502	30		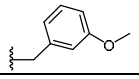	39.61	4.4021

[T]is the utilized test set compounds in CoMFA and CoMSIA.

field (March, 2019) [39];

- The system was neutralized by the addition of sodium and chloride (Na^+/Cl^-) ions;
- Using the steepest descent algorithm, the reduction in the system energy was exposed to 50,000 steps;
- The production of MD simulation was run for 20 ns for each simulation at a temperature of 300 k, a pressure of 1 bar, and a time step of 2 fs.

ADMET and Drug-Likeness Prediction

In silico ADMET prediction [40] is a crucial step in determining the pharmacokinetic and pharmacodynamic parameters and properties of molecules. These parameters are predicted by 3D-QSAR models and validated by molecular docking (MolPred 1-5) for it allows the identification of components needed to meet the minimal criteria of acceptance as potential medicinal components [20].

In this ADMET study, we used the online tools pkCSM [41] and SwissADME [42] to predict the ADMET properties of the four suggested molecules.

The ADMET study is based on the interpretation of the prediction results of the pharmacokinetic and pharmacodynamic properties. Accordingly, the obtained results must meet the following criteria:

- MW: Molecular weight must be under 500 DA (MW) < 500 Da;
- LogP: Water partition coefficient must be under 5 (logP) < 5;
- BBB level:
- Compounds with logBB values of 0.3 or higher that pass the blood-brain barrier instantly;
- Compounds with log BB values ranging from 0.3 to 1 that have access to the central nervous system (CNS);
- Compounds with log BB values of 1 that have a poor distribution to the brain.
- HIA (human intestinal absorption): The compound with an intestinal absorbance value that is higher than 30% is deemed to be extremely absorbed;
- CYP2D6: This is included in the metabolism of various substrates in the liver along with its inhibition by a drug constitute, mostly drug-drug interactions;
- Total clearance (Cltot): Drug clearance is defined by the rate constant and occurs mostly as a mix of renal clearance (excretion via the kidneys) and hepatic clearance (liver metabolism and biliary clearance). It is related to bioavailability and is critical in establishing dosage rates to achieve solid concentrations;
- AMES toxicity: It is a widely used technique for determining the mutagenic potential of a compound using bacteria. If the test is positive, it suggests the substance is mutagenic and may function as a carcinogen;
- Skin sensitization: This is a potential unfavorable effect for the products that are applied to the skin. A mandatory safety concern is the evaluation of the potential allergic contact dermatitis that could arise if the skin comes in contact with a compound.

RESULTS AND DISCUSSION

Database Alignment

The compilation of various compounds of the training and test sets in the distillation module of the Sybyl software revealed the common structure (core) of the training and test sets (Fig. 1).

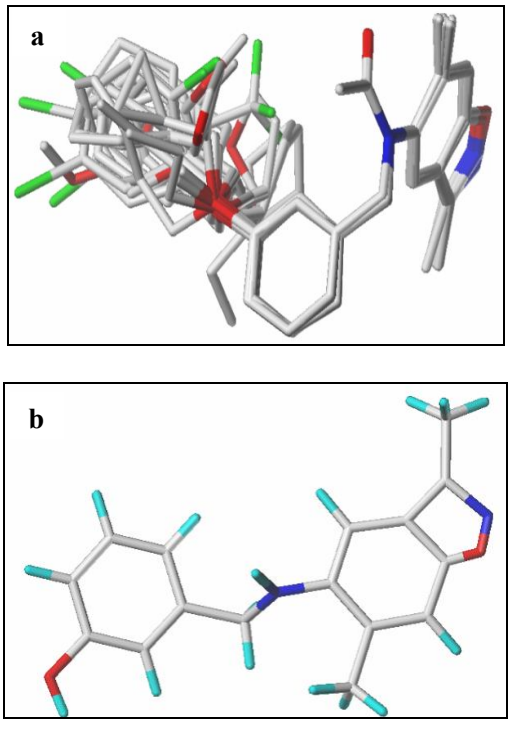

Fig. 1. Molecular alignment in the data set: (a) ligand-based alignment model of all the compounds; (b) molecular core.

Table 2. PLS Statistics of CoMFA and CoMSIA Models

Model	Q^2	R^2	SEE	F value	R^2 test	N	Filled distribution				
							STER	ELECT	ACC	DON	HYD
COMFA	0.781	0.997	0.040	945.249	0.700	6	0.594	0.406	-	-	-
COMSIA	0.793	0.935	0.184	41.067	0.729	6	0.633	-	-	0.367	-

The same PLS analysis was used in the final non-cross-validated analysis; R^2 = Non-cross-validated determination coefficient; R^2 test = External validation determination coefficient; SEE = Standard error of the estimate; F = Fischer value; N = Optimum number of components obtained from cross-validated; Q^2 = Cross-validated determination coefficient.

CoMFA and CoMSIA Results

Table 2 summarizes the statistical findings derived from the compilation of the CoMSIA and CoMFA system databases.

Table 3 and Figs. 2 and 3 show the observed and predicted pIC_{50} as well as their residues of CoMSIA and CoMFA.

The examination of the CoMFA model (electrostatic and steric fields) and CoMSIA (steric, hydrogen-bond donor fields) confirmed the validity of the statistical results, including R^2, Q^2, R^2 test, and SEE (Table 2).

It is worth noting that the CoMFA model consists of six main components, which is the optimal number of components given the number of molecules used in the development of this model. The values of correlation coefficient R^2 and cross-validation coefficient Q^2 were 0.997 and 0.781, respectively. The R^2 test resulted in a score of 0.700. These statistical results confirm the robustness of the CoMFA model.

Furthermore, the CoMSIA model is constructed using two basic primary components. Given the number of molecules employed in the construction of this model, this is the best option. The values of correlation coefficient R^2 and the cross-validation coefficient Q^2 were 0.793 and 0.935. The R^2 test resulted in a score of 0.729, suggesting that the CoMSIA model prediction was reliable.

A comparison of the CoMFA and CoMSIA models indicated that the CoMSIA results were extremely significant and could be utilized to predict novel TRIM24 bromodomain compounds with high potency action (Fig. 3). In the CoMFA model, the contributing fractions of each field showed that the steric and electrostatic fields shared fractions with 60% for the electrostatic fields and 40% for

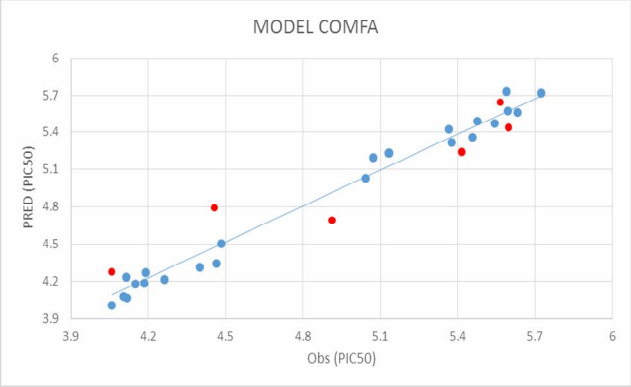

Fig. 2. CoMFA model: correlations between experimentally observed (pIC50) and predicted (pIC50) values for the test (red) and training (blue) sets of compounds.

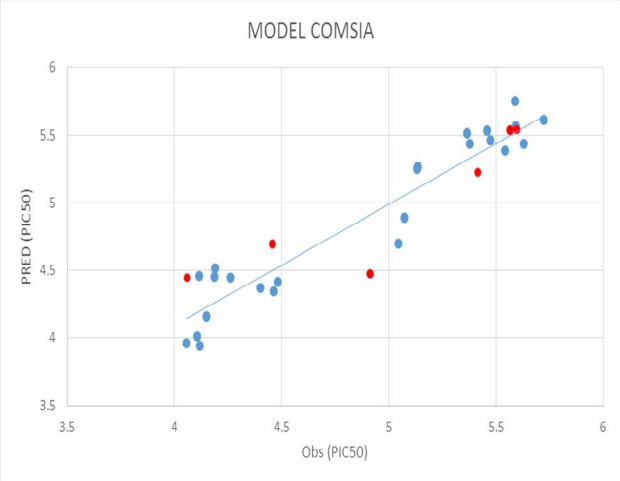

Fig. 3. CoMSIA model: correlations between experimentally observed (pIC50) and predicted (PIC50) values for the molecules of the test set (red color) and the training set (blue color).

Table 3. The Predicted and Observed Activity Values and the Residual Values Obtained by 3D-QSAR (CoMFA and CoMSIA)

Compound	pIC_{50} TRIM24 bromodomain	CoMFA pIC_{50}	Residual	CoMSIA pIC_{50}	Residual
1	5.1366	5.229	-0,0923	5.363	-0,2263
2	5.1325	5.229	-0,0965	5.205	-0,0725
3^{T}	5.4156	5.239	0,1767	5.245	0.1706
4	5.7258	5.718	0,0078	5.733	-0,0072
5	5.3777	5.310	0,0678	5.414	-0,0362
6	5.4762	5.488	-0,0117	5.416	0,0603
7	5.4596	5.357	0,1027	5.396	0,0637
8^{T}	5.5968	5.439	0,1579	5.412	0.184
9^{T}	4.9129	4.689	0,2239	4.007	0.905
10	5.5436	5.467	0,0766	5.501	0,0426
11	5.0452	5.026	0,0193	4.785	0,2603
12	5.3665	5.420	-0,0535	5.431	-0,0645
13	5.5951	5.573	0,0222	5.458	0,1372
14^{T}	5.5654	5.646	-0,0806	5.826	-0.2605
15	4.1502	4.177	-0,0268	4.127	0,0232
16	4.1059	4.069	0,0369	3.984	0,1219
17	4.1867	4.182	0,0048	4.388	-0,2012
18	4.1186	4.058	0,0607	3.956	0,1627
19	4.1168	4.231	-0,1142	4.390	-0,2732
20^{T}	4.6170	4.273	-0,2141	4.391	0.2260
21	4.0589	4.001	0,0579	3.892	0,1669
22	4.2636	4.211	0,0527	4.388	-0,1243
23	4.1909	4.265	-0,074	4.536	-0,345
24	5.0746	5.194	-0,1193	4.958	0,1167
25	5.5900	5.725	-0,1349	5.624	-0,0339
26	5.6326	5.561	0,0716	5.397	0,2356
27	4.4842	4.498	-0,0137	4.595	-0,1107
28	4.4661	4.335	0,1311	4.335	0,1311
29^{T}	4.4563	4.790	-0,3337	4.818	-0.3616
30	4.4021	4.308	0,0942	4.428	-0,0258

the steric fields. The steric fields and hydrogen acceptor percentages in the CoMSIA model were 63% and 37%, respectively.

Graphical Interpretation of Results Using CoMFA and CoMSIA

The ability to observe the zones in which the activity increases or decreases in the referential molecular structure is one of the advantages of the 3D-QSAR CoMSIA and CoMFA (compound 4). Following model compilation, the electrostatic and steric contour maps of CoMFA, as well as the hydrogen-bond donor and steric contour maps of CoMSIA, were all visible. The default contribution levels of 20% and 80% for the disfavored and favored locations,

respectively, were represented by outlines.

CoMFA Contour Maps

The red contour, which shows regions with increased activity and negative charges, and the blue contour, which shows sites where positive charges are favored, characterize the CoMFA electrostatic interactions. The yellow contour, which shows disfavored bulky substituents, and the green contour, which indicates favored bulky substituents, characterize the steric interactions of CoMFA. The results are illustrated in Figs. 4a and 4b.

A larger favorable green contour map nearby the position R2 (Fig. 4a) shows that the R_2 group is favorable in terms of steric field, which could explain why compound 4 (R2 = butyl; pIC_{50} = 5.725), was most active with compound 3 (R2 = propyl; pIC_{50} = 5.415), compound 2 (R2 = methyl; pIC_{50} = 5.1325), and compound 1 (R2 = hydrogen; pIC_{50} = 5.1366).

Furthermore, a small unfavorable yellow contour nearby the position R1 zone could explain why compound 1 (R1 = hydrogen; pIC_{50} = 5.1366) was most active with compound 27 (R1 = acetaldehyde; pIC_{50} = 4.484), and why compound **2** (R1 = methyl; pIC_{50} = 5.1325) was most active with compound 28 (R1 = acetaldehyde; pIC_{50} = 4.4661).

Figure 4b shows the electrostatic contour map. The blue contours show the regions where positive charges are favored. An elevated binding affinity on the substituent R2 represents a region in which the positive groups showed increased activity, explaining why compounds 1 (R1 = hydrogen; pIC_{50} = 5.1366) was most active with compound 27 (R1 = acetaldehyde; pIC_{50} = 4.484), and why compound 2 (R1 = methyl; pIC_{50} = 5.1325) was most active with compound 28 (R1 = acetaldehyde; pIC_{50} = 4.4661).

The red outlines, on the other hand, imply that the substituents must be rich in electrons. A strong binding affinity on the substituent R1 suggests the presence of a zone where negative groups and electron donors have improved activity. For example, compound 1 (R1 = hydrogen; pIC_{50} = 5.1366) was most active with compound 14 (R1 = 3-methylfuran; pIC_{50} = 5.565).

CoMSIA Contour Maps

In what follows, the focus is on steric (Fig. 5a) and acceptor (Fig. 5b) fields in CoMSIA contour maps.

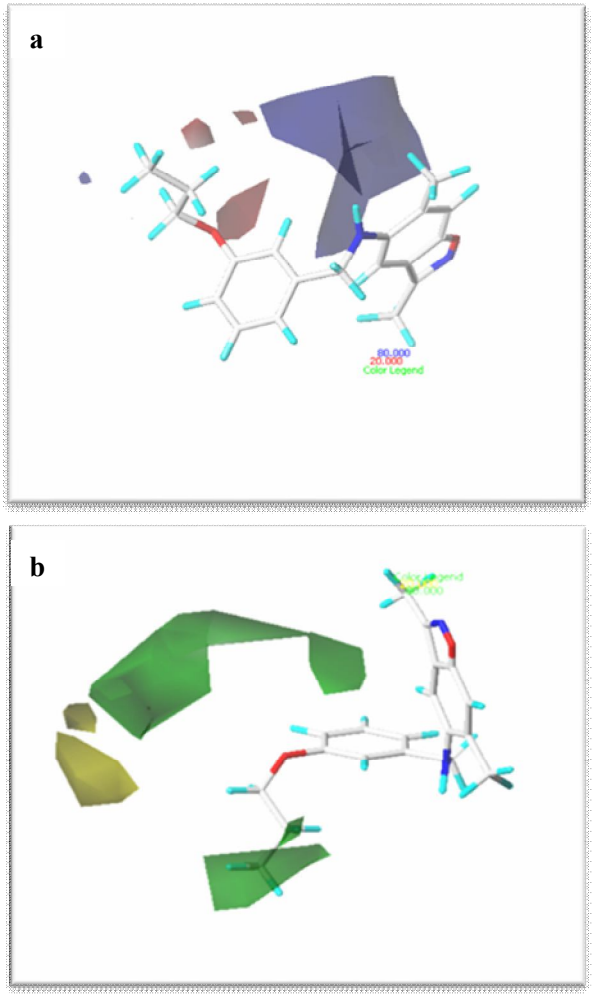

Fig. 4. Standardized coefficient contour maps of CoMFA analysis of the anti-cancer activity (compound 4).

A larger favorable green contour map close to the position R2 (Fig. 4a) indicates that the R2 group was favorable regarding the steric field, which could explain why compound 4 (R2 = butyl; pIC_{50} = 5.725) was most active with compound 3 (R2 = propyl; pIC_{50} = 5.415), compound 2 (R2 = methyl; pIC_{50} = 5.1325), and compound 1 (R2 = hydrogen; pIC_{50} = 5.1366),

In addition, a small unfavorable yellow contour nearby the position R1 zone explains why compound 1 (R1 = hydrogen; pIC_{50} = 5.1366) was most active with compound 27 (R1 = acetaldehyde; pIC_{50} = 4.484), and why compound 2 (R1 = methyl; pIC_{50} = 5.1325) was most active with compound 28 (R1 = acetaldehyde; pIC_{50} = 4.4661).

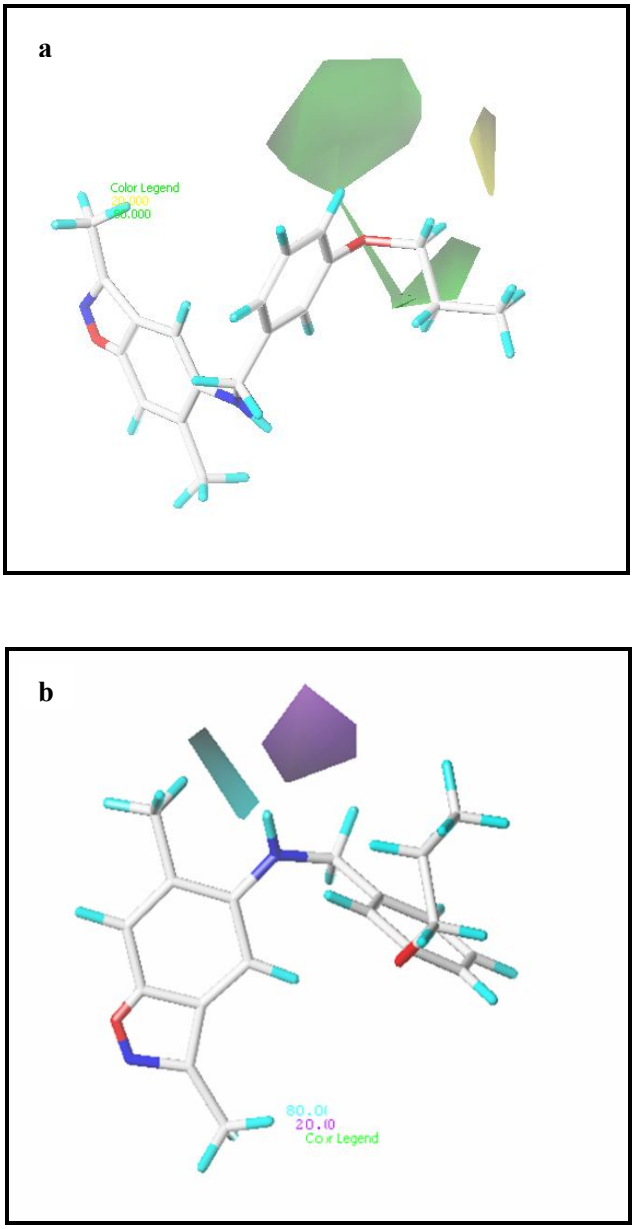

Fig. 5. (a) The steric fields: The green outlines depict locations where steric substituents improved the activity (80% contribution) whereas yellow contours depict areas where steric substituents reduced the activity (20%); (b) The acceptor-bond-donor field: The cyan outlines indicate areas where acceptor-bond-donor groups were more active (80% contribution) whereas the purple contours indicate areas where hydrogen-bond donor groups were less active (20% contribution).

The cyan contouring the R1 group reveals that a hydrogen-bond donor substituent in this area would increase activity. The purple contour reveals the importance of the hydrogen bonding acceptor group.

Docking Results

For the identification and detection of the proper placement of the active site of the TRIM24 bromodomain (PDB ID: 4YBT), the re-docking of the co-crystalized ligand was performed, as shown in Fig. 6. The results showed that the co-crystallized and re-docked fragments were closely coupled, suggesting that the docking process performed was reliable.

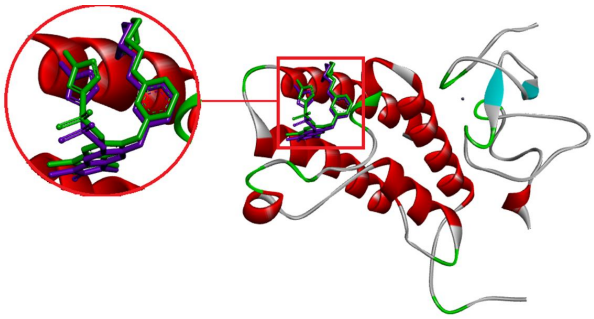

Fig. 6. Superposition of the re-docked ligand (purple stick) with the reference ligand (green stick) in the pocket TRIM24 bromodomain (PDB ID: 4YBT).

The docking study revealed the nature of the interaction between the series most active compound (compound 4) and the active site of the TRIM24 bromodomain protein (PDB ID: 4YBT) (Fig. 7).

According to the docking findings of compound 4, multiple types of ligands, as listed below, interacted with the active site of the TRIM24 bromodomain protein (Table 5):

Hydrogen bonds Try 935,

Pi-sigma bonds Val 896,

Pi-donor hydrogen bonds Asp 926. Asn 980. Pro 929. Val 928. Cys 976,

Pi-Alkyl bonds Val 932. Leu 922. Phe 924. Ala 932.

The multiplicity of interaction types between compound 4 and protein TRIM24 bromodomain explains the results indicating the low energy of the ligand (-6.46 kcal mol^{-1}).

Table 4. The Most Significant Interactions between the TRIM24 Bromodomain Site and Most Active Compounds Pred1

Compound	pIC_{50}	Pi-alkyl	Hydrogen bonds	Pi-donor hydrogen bonds	Pi-Sigma
4	5.7258	Val 932. Leu 922. Phe 924. Ala932	Try 935	Asp 926. Asn 980. Pro 929. Val 928. Cys 976	Val 896

Table 5. Compounds along with Their Structures and Predicted pIC50 based on 3D-QSAR (CoMSIA Model)

Compounds	pIC_{50} (Pred) of model CoMISA	Structure
MolPred 1	6.704	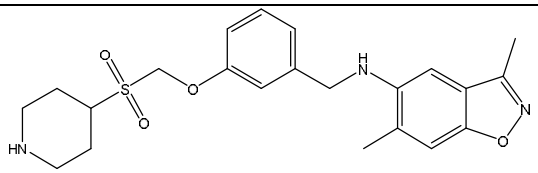
MolPred 2	6.041	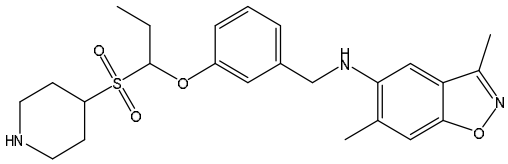
MolPred 3	5.956	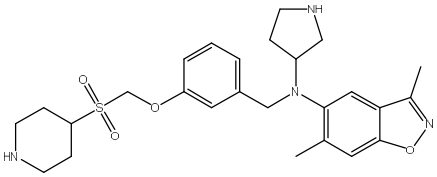
MolPred 4	5.829	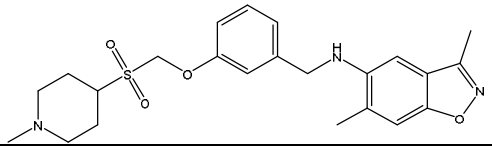

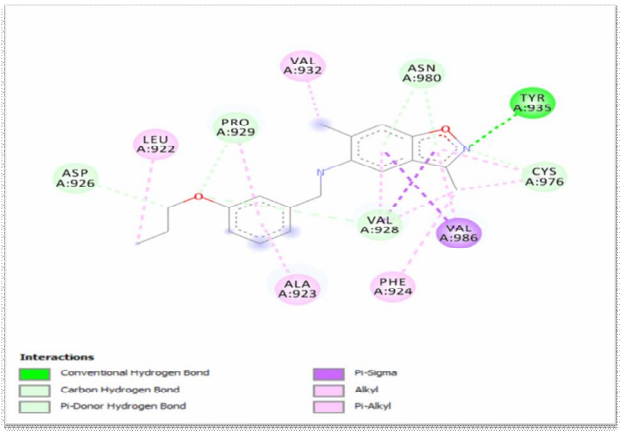

Fig. 7. Docking results of the interaction between compound 4 and TRIM24 bromodomain protein (PDB ID: 4YBT).

Design of New TRIM24 Bromodomain Inhibitors

The use of 3D-QSAR models and molecular docking to build novel TRIM24 bromodomain inhibitors with improved efficacy resulted in the development of new TRIM24 bromodomain inhibitors.

In this study, new TRIM24 bromodomain inhibitors are introduced based on 3D-QSAR and molecular docking data, which were optimized and aligned in the same way as the dataset compounds. The chemical structure and predicted activity levels of novel compounds, as well as the dataset pertinent to the strongest inhibitor, are displayed in Table 6. In terms of their activity, the newly developed compounds outperformed the most potent inhibitor in the collection.

We performed molecular docking using MolPred 1-4

Table 6. The Results of the Predicted Compounds Docking with TRIM24 Bromodomain Protein (PDB ID: 4YBT)

Compounds	Binding energy (kcal mol^{-1})	Docking result
MolPred 2	- 8.51	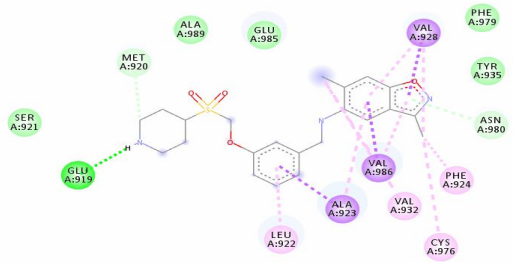
MolPred 3	- 8.43	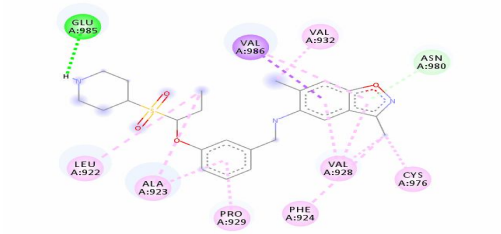
MolPred 4	- 7.96	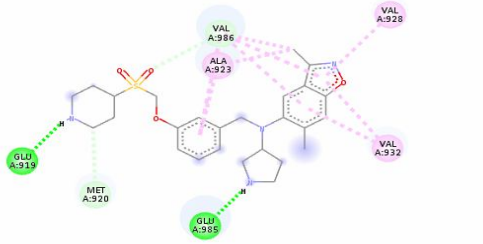
MolPred 5	- 7.70	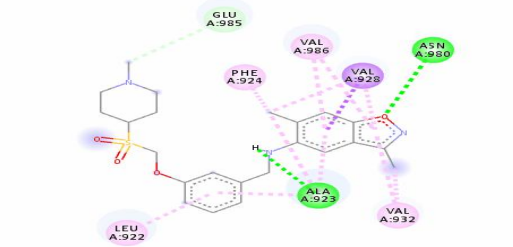

compounds to examine the types of liaisons and ligand constancy in the TRIM24 bromodomain enzyme (PDB ID: 4YBT), thus making sure that the suggested compounds were effective inhibitors. Table 7 shows the interactions between the predicted compounds and the TRIM24 bromodomain enzyme.

The findings showed that the binding energy of the predicted compounds in the active site of the TRIM24 bromodomain enzyme (PDB ID: 4YBT) was greater than that of the most powerful inhibitor in the dataset (-6.46 kcal mol^{-1}). This means that the novel compounds were more likely to bind with the TRIM24 bromodomain and have a substantial inhibitory impact on the TRIM24 bromodomain enzyme (PDB ID: 4YBT).

The ligand Predmol 1 has been resolved *via* four hydrogen bonds, particularly Glu919. A strong Pi-donor

Table 7. *In Silico* Prediction of Drug-likeness and ADMET Proprieties

No.	MW	HBA	HBD	logP	logS	HIA	BBB (logBB)	CYP 2D6 inhibition	Total Clearance	Toxicity		Drug-likeness	
										AMES	Skin Sensitization	Lipinski	Bioavailability Score
MolPred 1	457.590	7	2	4.338	-4.874	92.417	-0.538	No	0.653	No	No	Yes	0.55
MolPred 2	498.649	8	2	3.316	-4.03	90.759	-0.72	No	0.655	No	No	Yes	0.55
MolPred 3	443.569	7	1	3.902	-4.626	91.537	-0.546	No	0.669	No	No	Yes	0.55
MolPred 4	429.542	7	2	3.559	-4.386	90.832	-0.583	No	0.756	No	No	Yes	0.55

HBA = number of hydrogen bond acceptor MW = molecular weight, HIA = human intestinal absorption HBD = number of hydrogen bond donor, logP = octanol-water partition coefficient, logs = Water solubility, BBB = blood brain barrier.

hydrogen-bond interaction was produced between the residues of Met 920 and the newly designed 4-(ethylsulfonyl) piperidine group. The extra donor and hydrogen-bond interaction might explain the increased activity and docking affinity of compound Predmol 1.

ADMET Results

The results of the calculated ADMET molecular properties of predicted compounds (MOL1-4) are shown in Table 5. These results show that the predicted compounds had an adsorption value of the human intestines that varied between 90.75% and 92.41%, suggesting excellent adsorption of these compounds by the intestines and hence their efficiency in acting quickly.

Regarding the blood-brain barrier value, it was observed that the value of Log BB was less than 1, which means that the compounds were not transmitted to the brain; thus, the central nervous system (CNS) was protected.

At the level of CYP2D6 metabolism, the predicted compounds did not inhibit CYP2D6, which plays a vital role in the degradation of excess drugs in the body.

The results of the total clearance, expressed in $\log Ct_{tot}$, showed that the liver was capable of breaking down the molecules slowly, leaving enough time for the predicted drugs to act in the body.

The toxicity of the predicted compounds was measured by the AMES parameter, which indicated that not all compounds were toxic.

To sum up, it can be concluded that the results of the *in silico* ADMET properties indicated that the pharmacokinetic and pharmacodynamic properties of the predicted molecules (MolPred 1-4) were reliable; therefore, these compounds can be used as potential drugs against prostate cancers.

Molecular Dynamic Simulation

Compounds 4 and Pred1 were submitted to MD simulation to confirm the results of molecular docking and the stability of docked compounds in the binding site of TRIM24 bromodomain protein (PDB ID: 4YBT). All systems were utilized for a 20 ns time scale simulation.

Figure 8a shows the root-mean-square-deviation (RMSD) of the 4YBT-Mol4 and 4YBT-Pred1 complexes. The average RMSD values of the 4YBT-Mol4 and 4YBT-Pred1 systems were 0.31 and 0.21 nm, respectively. As a result, the complex 4YBT F Pred1 had a more stable structure than the complex 4YBT-Mol4.

Root-mean-square fluctuations (RMSFs) of C atoms in TRIM24 (PDB ID: 4YBT) were estimated based on the final 40 ns of MD trajectories to investigate the influence of inhibitor bindings on the structural fluctuation of TRIM24. As shown in Fig. 8b, except for the region near residues 864 and 887, the RMSF values basically decreased due to the binding of inhibitors to TRIM24 (PDB ID: 4YBT), which suggests that the presence of inhibitors restricted the fluctuation of certain residues from TRIM24 (PDB ID: 4YBT). In addition, the Pred1 binding increased structural fluctuation near residues 864 and 887, which indicates that the substitutions hinge-binding scaffold produced perturbation in the flexibility of this region.

We also used the radius of gyration and solvent accessible surface area analysis to determine the compaction

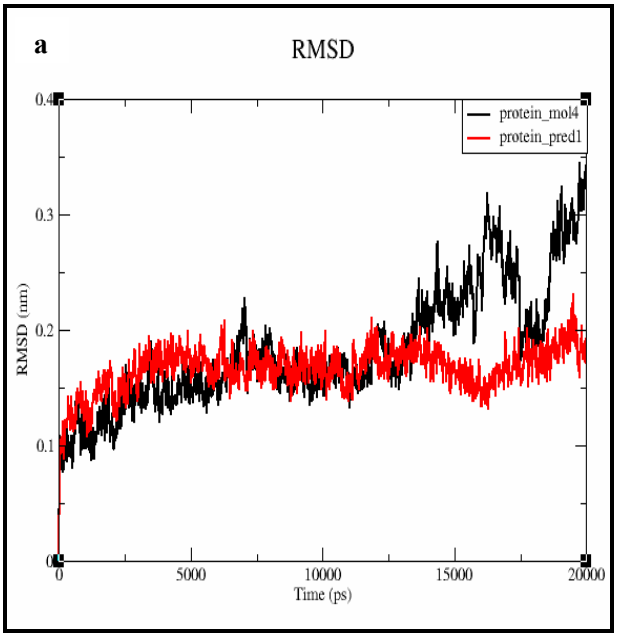

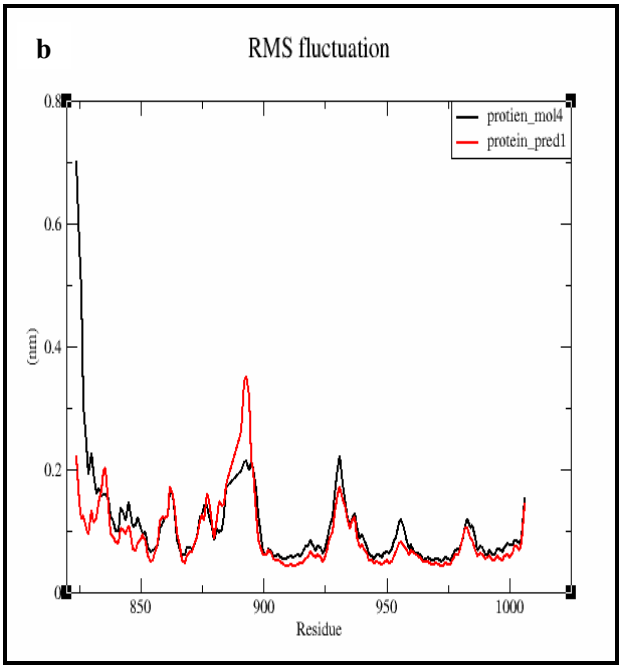

Fig. 8. Molecular dynamics simulations: (a) RMSD of backbone over the 20 ns of MD simulation at 300 K and 1 bar; (b) RMSF of residues during MD simulation. In both figures, the red color represents the 4YBT-Mol4 complex, and the black color represents the 4YBT-Pred1 complex.

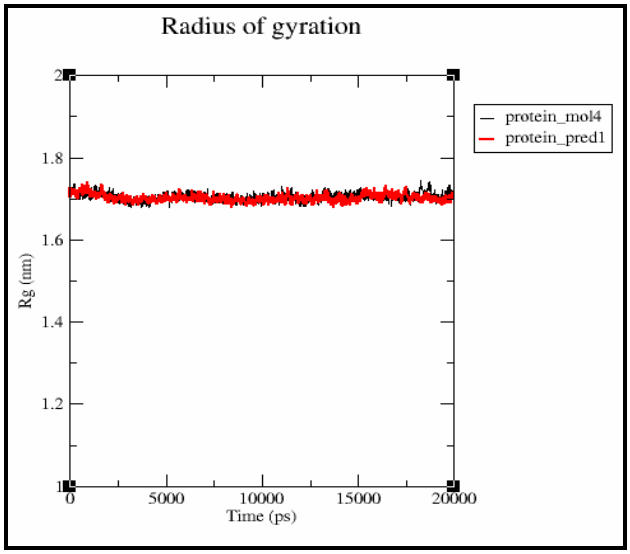

Fig. 9. The radius of gyration corresponds to 10 ns MD simulation at 300 K. The red color represents the 4YBT-Mol4 complex, and the black color represents the 4YBT-Pred1 complex.

level in TRIM24 (PDB ID: 4YBT) and the structure of compounds Mol4 and Pred1. The analysis of the radius of gyration provided an insight into the overall dimensions of the protein. Figure 9 illustrates the plot of Rg 4YBT-Mol4 and 4YBT-Pred1 complexes for 10 ns simulation time at 300 K. The radius of gyration (Rg) of 4YBT-Mol4 and 4YBT-Pred1 was found to be 1.72 and 1.71 nm, respectively. Throughout the simulation period, the curve demonstrated that 4YBT-Mol4 had a larger Rg value than 4YBT-Pred1. As a result, it can be concluded that 4YBT-Pred1 improves enzyme stability.

As clearly indicated in Fig. 10, the main secondary structural components of the ligand and protein in the TRIM24 bromodomain protein (PDB ID: 4YBT) complex remained relatively similar to their original configuration before the MD simulation. Figure 10 also shows that all the ligands bound to the position close to the initial binding site. All of these results are in agreement with those obtained by 3D-QSAR and molecular docking.

CONCLUSIONS

In this research, 3D-QSAR and molecular docking were

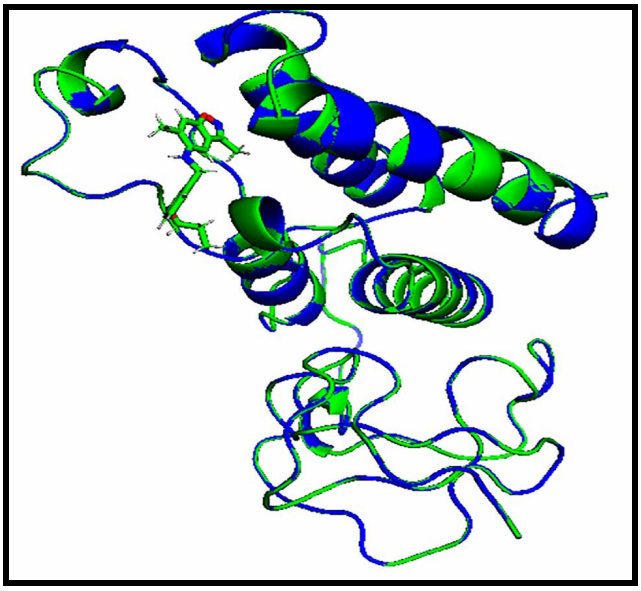

Fig. 10. The superposition of the final complex structure after MD simulation for 20 ns (green color) and initial complex structures before MD simulation (blue color).

used to predict the anti-cancer activities of a series of N-benzyl-3,6-dimethylbenzo[d]-isoxazol-5-amine derivatives as potential inhibitors of (TRIM24) bromodomain in prostate cancers. The 3D-QSAR models were developed using a PLS model, which included CoMFA and CoMSIA. All of the developed models were found to have excellent R2, Q2, and R2 test values, indicating that the models were statistically reliable. Molecular docking was used to explore the binding site interactions and energy between ligands and the (TRIM24) bromodomain protein. The findings were consistent with those obtained by the 3D-QSAR model. Four new N-benzyl-3,6-dimethylbenzo[d]-isoxazol-5-amine derivatives were predicted using CoMSIA. The results of the docking study indicated that these predicted compounds were more stable in the binding pocket of the (TRIM24) bromodomain receptor than the most powerful inhibitor in the dataset (compound 4), and their pharmacokinetic characteristics were confirmed by drug-likeness and ADMET prediction. The results of MD simulation also showed that compound Pred1 was stable in the binding pocket of (TRIM24) bromodomain receptor during the 20 ns of simulation time.

FUNDING

This research received no funding.

ACKNOWLEDGMENTS

The authors would like to thank the Moroccan Association of Theoretical Chemistry (MATC) for its help regarding the software used in this study.

CONFLICTS OF INTEREST

All authors declare that they have no conflicts of interest in this article.

REFERENCES

[1] Niraula, S.; Chi, K.; Joshua, A. M., Beyond castration-defining future directions in the hormonal treatment of prostate cancer. *Hormones and Cancer* **2012**, *3*, 3-13, DOI: 10.1007/s12672-011-0096-0.

[2] Davies, A.; Conteduca, V.; Zoubeidi, A.; Beltran, H., Biological evolution of castration-resistant prostate cancer. *Eur. Urol. Focus* **2019**, *5*, 147-154, DOI: 10.1016/j.euf.2019.01.016.

[3] Shafi, A. A.; Yen, A. E.; Weigel, N. L., Androgen receptors in hormone-dependent and castration-resistant prostate cancer. *Pharmacol. Therapeut.* **2013**, *140*, 223-238, DOI: 10.1016/j.pharmthera.2013.07.003.

[4] Ingrosso, G.; Detti, B.; Scartoni, D.; Lancia, A.; Giacomelli, I.; Baki, M.; Carta, G.; Livi, L.; Santoni, R., Current therapeutic options in metastatic castration-resistant prostate cancer. *Semin. Oncol.* **2018**, *45*, 303-315, DOI: 10.1053/j.seminoncol.2018.10.001.

[5] Wang, J.; Zou, J.X.; Xue, X.; Cai, D.; Zhang, Y.; Duan, Z.; Xiang, Q.; Yang, J. C.; Louie, M. C.; Borowsky, A. D.; *et al.*, ROR-γ drives androgen receptor expression and represents a therapeutic target in castration-resistant prostate cancer. *Nat. Med.* **2016**, *22*, 488-496, DOI: 10.1038/nm.4070.

[6] Zhang, M.; Zhang, Y.; Song, M.; Xue, X.; Wang, J.; Wang, C.; Zhang, C.; Li, C.; Xiang, Q.; Zou, L.; *et al.*,

Structure-based discovery and optimization of benzo [d] isoxazole derivatives as potent and selective BET inhibitors for potential treatment of castration-resistant prostate cancer (CRPC). *J. Med. Chem.* **2018**, *61*, 3037-3058, DOI: 10.1021/ acs.jmedchem.8b00103.

[7] Xiang, Q.; Wang, C.; Zhang, Y.; Xue, X.; Song, M.; Zhang, C.; Li, C.; Wu, C.; Li, K.; Hui, X.; *et al.*, Discovery and optimization of 1-(1H-indol-1-yl)ethanone derivatives as CBP/EP300 bromodomain inhibitors for the treatment of castration-resistant prostate cancer. *Eur. J. Med. Chem.* **2018**, *147*, 238-252, DOI: 10.1016/j.ejmech.2018.01.087.

[8] Stone, L., TRIM24 acts as a transcriptional activator. *Nat. Rev. Urol.* **2016**, *13*, 437, DOI: 10.1038/ nrurol.2016.112.

[9] Hatakeyama, S., TRIM proteins and cancer. *Nat. Rev. Cancer* **2011**, *11*, 792-804, DOI: 10.1038/ nrc3139.

[10] Hatakeyama, S. TRIM family proteins: Roles in autophagy, immunity, and carcinogenesis. *Trends Biochem. Sci.* **2017**, *42*, 297-311, DOI: 10.1016/ j.tibs.2017.01.002.

[11] Meroni, G., TRIM E3 ubiquitin ligases in rare genetic disorders. *Adv. Exp. Med. Biol.* **2020**, *1233*, 311-325, DOI: 10.1007/978-3-030-38266-7_14.

[12] Appikonda, S.; Thakkar, K. N.; Barton, M. C., Regulation of gene expression in human cancers by TRIM24. *Drug Discov. Today: Technologies* **2016**, *19*, 57-63, DOI: 10.1016/j.ddtec.2016.05.001.

[13] Filippakopoulos, P.; Picaud, S.; Mangos, M.; Keates, T.; Lambert, J. P.; Barsyte-Lovejoy, D.; Felletar, I.; Volkmer, R.; Müller, S.; Pawson, T.; *et al.*, Histone recognition and large-scale structural analysis of the human bromodomain family. *Cell* **2012**, *149*, 214-231, DOI: 10.1016/j.cell.2012.02.013.

[14] Patel, L. R.; Barton, M. C., TRIM-ing ligand dependence in castration-resistant prostate cancer. *Cancer Cell* **2016**, *29*, 776-778, DOI: 10.1016/ j.ccell.2016.05.014.

[15] Groner, A. C.; Cato, L.; de Tribolet-Hardy, J.; Bernasocchi, T.; Janouskova, H.; Melchers, D.; Houtman, R.; Cato, A. C. B.; Tschopp, P.; Gu, L.; *et al.,* TRIM24 Is an oncogenic transcriptional activator in prostate cancer. *Cancer Cell* **2016**, *29*, 846-858, DOI: 10.1016/j.ccell.2016.04.012.

[16] Gechijian, L. N.; Buckley, D. L.; Lawlor, M. A.; Reyes, J. M.; Paulk, J.; Ott, C. J.; Winter, G. E.; Erb, M. A.; Scott, T. G.; Xu, M.; *et al.*, Functional TRIM24 degrader *via* conjugation of ineffectual bromodomain and VHL ligands. *Nat. Chem. Biol.* **2018**, *14*, 405-412, DOI: 10.1038/s41589-018-0010-y.

[17] Hu, Q.; Wang, C.; Xiang, Q.; Wang, R.; Zhang, C.; Zhang, M.; Xue, X.; Luo, G.; Liu, X.; Wu, X.; *et al.*, Discovery and optimization of novel N-benzyl-3,6-dimethylbenzo[d]isoxazol-5-amine derivatives as potent and selective TRIM24 bromodomain inhibitors with potential anti-cancer activities. *Bioorg. Chem.* **2020**, *94*, 103424, DOI: 10.1016/ j.bioorg.2019.103424.

[18] Chhatbar, D. M.; Chaube, U. J.; Vyas, V. K.; Bhatt, H. G., CoMFA, CoMSIA, Topomer CoMFA, HQSAR, molecular docking and molecular dynamics simulations study of triazine morpholino derivatives as mTOR inhibitors for the treatment of breast cancer. *Comput. Biol. Chem.* **2019**, *80*, 351-363, DOI: 10.1016/j.compbiolchem.2019.04.017.

[19] Goudzal, A.; El Aissouq, A.; El Hamdani, H.; Ouammou, A., QSAR modeling, molecular docking studies and ADMET prediction on a series of phenylaminopyrimidine-(thio) urea derivatives as CK2 inhibitors. *Materials Today: Proceedings* **2020**, *51*, 1851-1862, DOI: 10.1016/ j.matpr.2020.08.044.

[20] Oussama, C.; Abdellah, E. A.; Youssef, E. O.; Mohammed, B.; Abdelkrim, O., *In silico* prediction of novel sars-cov 3cl pro inhibitors: A combination of 3d-qsar, molecular docking, admet prediction, and molecular dynamics simulation. *Biointerface Res. Appl. Chem.* **2022**, *12*, 5100-5115, DOI: 10.33263/BRIAC124.51005115.

[21] Olasupo, S. B.; Uzairu, A.; Shallangwa, G.; Uba, S., QSAR modeling, molecular docking and ADMET/pharmacokinetic studies: a chemometrics approach to search for novel inhibitors of norepinephrine transporter as potent antipsychotic drugs. *J. Iran. Chem. Soc.* **2020**, *17*, 1953-1966, DOI: 10.1007/s13738-020-01902-5.

[22] Osman, E. A.; Abdalla, M. A.; Abdelraheem, M. O.;

Ali, M. F.; Osman, S. A.; Tanir, Y. M.; Abdelrahman, M.; Ibraheem, W.; Alzain, A. A., Design of novel coumarins as potent Mcl-1 inhibitors for cancer treatment guided by 3D-QSAR, molecular docking and molecular dynamics. *Informatics in Medicine Unlocked* **2021**, *26*, 100765, DOI: 10.1016/j.imu.2021.100765.

[23] El McHichi, L.; El Aissouq, A.; Kasmi, R.; Belhassan, A.; El-Mernissi, R.; Ouammou, A.; Lakhlifi, T.; Bouachrine, M., *In silico* design of novel Pyrazole derivatives containing thiourea skeleton as anti-cancer agents using: 3D QSAR, Drug-Likeness studies, ADMET prediction and molecular docking. *Materials Today: Proceedings* **2021**, *45*, 7661-7674, DOI: 10.1016/J.MATPR.2021.03.152.

[24] Chedadi, O.; El Aissouq, A.; El Ouardi, Y.; Bouachrine, M.; Ouammou, A., 3D-QSAR and molecular docking studies of 4-methyl quinazoline derivatives as PI3Kα inhibitors. *J. Indian Chem. Soc.* **2021**, *98*, 100183, DOI: https://doi.org/10.1016/j.jics.2021.100183.

[25] Gasteiger, J.; Saller, H., Calculation of the charge distribution in conjugated systems by a quantification of the resonance concept. *Angewandte Chemie International Edition in English* **1985**, *24*, 687-689, DOI: 10.1002/anie.198506871.

[26] Wu, S.; Qi, W.; Su, R.; Li, T.; Lu, D.; He, Z., CoMFA and CoMSIA analysis of ACE-inhibitory, antimicrobial and bitter-tasting peptides. *Eur. J. Med. Chem.* **2014**, *84*, 100-106, DOI: 10.1016/j.ejmech.2014.07.015.

[27] Pirhadi, S.; Shiri, F.; Ghasemi, J. B., Pharmacophore elucidation and 3D-QSAR analysis of a new class of highly potent inhibitors of acid ceramidase based on maximum common substructure and field fit alignment methods. *J. Iran. Chem. Soc.* **2014**, *11*, 1329-1336, DOI: 10.1007/s13738-013-0402-6.

[28] Begum, S.; Jaswanthi, P.; Venkata Lakshmi, B.; Bharathi, K., QSAR studies on indole-azole analogues using DTC tools; imidazole ring is more favorable for aromatase inhibition. *J. Indian Chem. Soc.* **2021**, *98*, 100016. DOI: 10.1016/j.jics.2021.100016.

[29] Stitou, M.; Toufik, H.; Bouachrine, M.; Lamchouri, F., Quantitative structure-activity relationships analysis, homology modeling, docking and molecular dynamics studies of triterpenoid saponins as Kirsten rat sarcoma inhibitors. *J. Biomol. Struct. Dyn.* **2020**, *1102*, 152-170, DOI: 10.1080/07391102.2019.1707122.

[30] Yang, H.; Xie, W.; Xue, X.; Yang, K.; Ma, J.; Liang, W.; Zhao, Q.; Zhou, Z.; Pei, D.; Ziebuhr, J.; *et al.*, Design of wide-spectrum inhibitors targeting coronavirus main proteases. *PLoS Biology* **2005**, *3*, DOI: 10.1371/journal.pbio.0030324.

[31] Palmer, W. S.; Poncet-Montange, G.; Liu, G.; Petrocchi, A.; Reyna, N.; Subramanian, G.; Theroff, J.; Yau, A.; Kost-Alimova, M.; Bardenhagen, J. P.; *et al.*, Structure-guided design of IACS-9571, a selective high-affinity dual TRIM24-BRPF1 bromodomain inhibitor. *J. Med. Chem.* **2016**, *59*, 1440-1454, DOI: 10.1021/acs.jmedchem.5b00405.

[32] Berman, H. M.; Westbrook, J.; Feng, Z.; Gilliland, G.; Bhat, T. N.; Weissig, H.; Shindyalov, I. N.; Bourne, P. E., The protein data bank. *Nucleic Acids Research* **2000**, *28*, 235-242, DOI: 10.1093/nar/28.1.235.

[33] Trott, O.; Olson, A. J., Software news and update AutoDock Vina : Improving the speed and accuracy of docking with a new scoring function, efficient optimization, and multithreading. *J. Comput. Chem.* **2009**, *31*, 455-461, DOI: 10.1002/jcc.

[34] Schrödinger, LLC The {PyMOL} Molecular Graphics System, Version~1.8; **2015**.

[35] Discovery Studio Predictive Science Application | Dassault Systèmes BIOVIA Available online: https://www.3dsbiovia.com/products/collaborative-science/biovia-discovery-studio/ (accessed on Jan 28, **2020**).

[36] Briones, R.; Blau, C.; Kutzner, C.; de Groot, B. L.; Aponte-Santamaría, C., GROmaps: A GROMACS-based toolset to analyze density maps derived from molecular dynamics simulations. *Biophys. J.* **2019**, *116*, 4-11, DOI: 10.1016/j.bpj.2018.11.3126.

[37] Vanommeslaeghe, K.; Hatcher, E.; Acharya, C.; Kundu, S.; Zhong, S.; Shim, J.; Darian, E.; Guvench, O.; Lopes, P.; Vorobyov, I.; Mackerell Jr., A. D., CHARMM general force field: A force field for drug-like molecules compatible with the CHARMM all-atom additive biological force fiel ds. *J. Comput.*

Chem. **2010**, *31*, 671-690, DOI: https://doi.org/10.1002/jcc.21367.

[38] Jorgensen, W. L.; Chandrasekhar, J.; Madura, J. D.; Impey, R. W.; Klein, M. L., Comparison of simple potential functions for simulating liquid water Comparison of simple potential functions for simulating liquid water. *J. Chem. Phys.* **1983**, *7,* 962, DOI: 10.1063/1.445869.

[39] Best, R. B.; Zhu, X.; Shim, J.; Lopes, P. E. M.; Mittal, J.; Feig, M.; Mackerell, A. D., Optimization of the additive CHARMM all-atom protein force field targeting improved sampling of the backbone ϕ , ψ and side-chain χ 1 and χ 2 dihedral angles. *J. Chem. Theory Comput.* **2012**, *8*, 3257-3273, DOI: https://doi.org/10.1021/ct300400x.

[40] Nainwal, L. M.; Shaququzzaman, M.; Akhter, M.; Husain, A.; Parvez, S.; Khan, F.; Naematullah, M.; Alam, M. M., Synthesis, ADMET prediction and reverse screening study of 3,4,5-trimethoxy phenyl ring pendant sulfur-containing cyanopyrimidine derivatives as promising apoptosis inducing anticancer agents. *Bioorg. Chem.* **2020**, *104*, 104282, DOI: 10.1016/j.bioorg.2020.104282.

[41] Pires, D. E. V.; Blundell, T. L.; Ascher, D. B., pkCSM: Predicting small-molecule pharmacokinetic and toxicity properties using graph-based signatures. *J. Med. Chem.* **2015**, *58*, 4066-4072, DOI: 10.1021/acs.jmedchem.5b00104.

[42] Daina, A.; Michielin, O.; Zoete, V., SwissADME: A free web tool to evaluate pharmacokinetics, drug-likeness and medicinal chemistry friendliness of small molecules. *Sci. Reports* **2017**, *7*, 1-13, DOI: 10.1038/srep42717.